Horizontal Sustained Force Delivery with an Aerial Manipulator using Hybrid Force/Position Control

Hameed Ullah, Simone D'Angelo, Fabio Ruggiero, Vincenzo Lippiello
Department of Electrical Engineering and Information Technology
University of Naples Federico II,
Naples, Italy
ORCID: 0000-0002-4022-9657, 0000-0001-5658-7486,
0000-0001-7539-9157, 0000-0002-6089-2333

Santos Miguel Orozco Soto
Science and Technology College
Autonomous University of Mexico City
Mexico City, Mexico
ORCID: 0000-0001-6191-4306
santos.orozco@uacm.edu.mx

***Abstract*—This paper introduces a novel hybrid force/position control system tailored for aerial manipulators, aiming to enable efficient and sustained delivery of horizontal forces. Unlike existing approaches mainly designed for ground-fixed manipulators, this architecture is specifically developed for aerial robotics. By leveraging physics-engine based simulations, the proposed system demonstrates effectiveness in generating large controlled forces over extended periods, improving comparable hybrid controllers documented in the literature. These findings offer valuable insights for optimizing aerial manipulators, particularly in scenarios necessitating prolonged horizontal force exertion. The study's contributions hold promise for various applications, including search and rescue operations, infrastructure maintenance, and environmental monitoring, thereby driving advancements in aerial manipulation technologies.**

***Index Terms*—Aerial manipulators, controlled force delivery, hybrid position/force control, actively tilting quadrotors.**

I. Introduction

Unmanned Aerial Vehicles (UAVs) have become integral across various applications, benefiting from their versatility, maneuverability, and cost-effectiveness. Their utility spans from cinematography to critical infrastructure inspections and environmental monitoring, expanding to include tasks once deemed inaccessible or hazardous for humans [1]–[3]. However, a significant limitation arises when these UAVs need to actively interact with their surroundings [1].

To address these constraints, UAVs have transitioned from passive tasks to active ones that involve manipulation and physical interactions with the environment. These active tasks encompass a wide range of activities, including push and slide operations, peg-in-hole tasks, grasping, picking and placing objects, transportation, positioning, construction, demolition, cleaning tall buildings, and working in hazardous environments. This transition necessitates equipping drones with manipulative capabilities, often in the form of robotic arms or attached tools. This integration, known as aerial manipulation, enables UAVs to perform a wide array of tasks, from infrastructure maintenance to disaster response [1], [4]–[6]. This shift towards active tasks involves outfitting drones with robotic manipulators featuring multiple degrees of freedom (DoF) [7] or employing a mounted stick [8]. This integration of manipulative capabilities, often referred to as an aerial manipulator [1], [6], has enabled UAVs to expand their utility across various applications.

Nevertheless, stabilizing aerial manipulators while performing physical tasks poses significant control challenges, especially in delivering controlled forces to the environment. Various control techniques have been explored in the literature, including nonlinear disturbance-observer-based robust controllers [9], model predictive controllers [10], and impedance control [6]. However, achieving sustained large forces over extended periods remains elusive. Only a few report the achievement of larger forces than 5 N for long periods, whether in simulation or actual experiments, which is usually required for several applications.

This paper introduces a novel hybrid position/force control architecture for aerial manipulators, capitalizing on the tilting rotor's capability to exert horizontal forces. The proposed control system enables the sustained delivery of up to 8 N of force for several minutes, surpassing previous state-of-the-art approaches [11]. The system is implemented in C++ and Python, with communication facilitated by the Robot Operating System (ROS) middleware. The experiments were carried out in the *Gazebo* physics-engine-based simulator using a virtual version of the aerial manipulator, which represents an advantage concerning the traditional numerical simulation due to the several physical phenomena included by default, yielding closer-to-reality results.

The remainder of the paper is organized as follows: Section II presents the dynamical model of the aerial manipulator, followed by the design of the hybrid force/position controller in Section III. Section IV details the simulation results, and finally, the conclusion summarizes the contributions of the study.

II. Aerial Manipulator Dynamics

To analyze the dynamics of a closed-loop controlled system effectively, a comprehensive understanding of its dynamics is crucial. While the generalized dynamical model of an aerial manipulator is available in the literature, specifically in [6], this study focuses on an aerial manipulator with a static robotic

978-8-3503-5070-8/24/$31.00 ©2024 IEEE

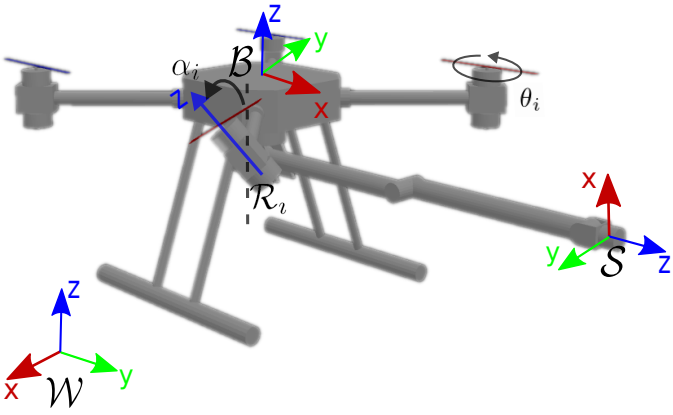

Fig. 1: Omnidirectional tilting quadrotor equipped with a sensorized stick. The main frames are depicted.

arm, simplifying the system dynamics significantly. In this scenario, the aerial manipulator can be described as a 6-degree-of-freedom flying rigid object. The schematic diagram in Fig. 1 illustrates the actively tilting aerial manipulator, with frames labeled as F_W for the world frame, F_B for the body reference frame, and F_R for the propellers reference frame. The position of the aerial manipulator is represented by ${}^W p_B = [x_B \ y_B \ z_B]^T$, and its orientation is expressed as ${}^W \eta_B = [\phi_B \ \theta_B \ \psi_B]^T$, denoting roll, pitch, and yaw, respectively. Thus, the dynamic analysis of the actively tilting quadrotor with a static robotic arm involves Newton–Euler formulation and algebraic computations. The dynamic equation is given by:

$$B(\zeta)\ddot{\zeta} + C(\zeta, \dot{\zeta})\dot{\zeta} + g(\zeta) = G_B(\zeta)u_B, \tag{1}$$

where, $\zeta \in \mathbb{R}^6 \triangleq \left[{}^W p_B{}^T \ {}^W \eta_B{}^T\right]^T$ represents the six-dimensional pose of the UAV w.r.t. the world frame W, $g(\zeta) \in \mathbb{R}^6$ is the gravity force vector, and $B(\zeta) \in \mathbb{R}^{6\times 6}$ is the inertia matrix represented as

$$B(\zeta) = \begin{bmatrix} mI_{3\times 3} & 0_{3\times 3} \\ 0_{3\times 3} & D\left({}^W \eta_B\right) \end{bmatrix},$$

with $I_{3\times 3}$ and $0_{3\times 3}$ denoting the identity and zero matrices of the specified dimensions, $D({}^W \eta_B) \in \mathbb{R}^{3\times 3}$ is the inertia matrix of the angular part and m is the total UAV mass. Moreover, $D\left({}^W \eta_B\right) = E\left({}^W \eta_B\right)^T J_B E\left({}^W \eta_B\right)$, where J_B is the inertia tensor of the airframe, and $E(\eta_B) \in \mathcal{SO}(3)$ is a rotation matrix [12]. The matrix $C(\zeta, \dot{\zeta})$ represents the centrifugal and Coriolis forces, and it is given by

$$C(\zeta, \dot{\zeta}) = \begin{bmatrix} 0_{3\times 3} & 0_{3\times 3} \\ 0_{3\times 3} & \begin{array}{c} E({}^W \eta_B)^T S_\times \left(E({}^W \eta_B){}^W \dot{\eta}_B\right) J_b E({}^W \eta_B) \\ + E({}^W \eta_B)^T J_b \dot{E}({}^W \eta_B) \end{array} \end{bmatrix},$$

where $S_\times$ represents the skew-symmetric operator. In addition, $G_B(\zeta) = \text{blockdiag}\left(R({}^W \eta_B), E({}^W \eta_B)\right)$, with $R({}^W \eta_B) \in \mathcal{SO}(3)$ denoting the rotation matrix from W to B [12].

It is important to note that the symmetric, positive definite, and invertible nature of the matrix $B(\zeta)$ is maintained within specific maneuvers due to the "X" configuration of the actively tilting quadrotor. This characteristic makes it suitable for translational motions, as demonstrated in [12]. Additionally, we assume that an accurate measurement of the full pose ζ is available for our analysis.

A. Thrust Vectoring

An important feature of an actively tilting quadrotor is its capability to exert horizontal thrust, which turns it into an omnidirectional UAV within some orientation range. Consider Fig. 1, where a rotor frame R_i is illustrated. For standard non tilitng quadotors, each rotor is only capable of exerting thrust $T_i \in \mathbb{R}$ along z_i, whereas such a thrust can be decomposed (vectored) in $T_i \in \mathbb{R}^2 \triangleq [T_{i_{xy}} \ T_{i_z}]^T = [T_i \sin(\alpha_i) \ T_i \cos(\alpha_i)]^T$ when actively rotating the rotors α_i units about ${}^B x_{R_i}$ axis by means of servomotors. As aforementioned, this thrust vectoring enables the UAV to move along ${}^W x_B$ and ${}^W y_B$ directions without changing its *roll* and *pitch* angles, and consequently it is capable to deliver horizontal force by mapping the x and y control input components to desired vectored thrusts.

B. Control Allocation

Consider again Fig. 1, the position ${}^B p_{R_i} \in \mathbb{R}^3$ and orientation ${}^B R_{R_i}(\alpha_i(t)) \in SO(3)$ of the coordinate frame of each rotor concerning the airframe are

$${}^B p_{R_i} = \begin{bmatrix} x_{R_i} & y_{R_i} & z_{R_i} \end{bmatrix}^T = L R_z(\chi_i)\mathbf{e}_1, \tag{2}$$

$${}^B R_{R_i}(\alpha_i(t)) = R_z(\chi_i) R_x(\alpha_i(t)), \tag{3}$$

with $i = 1, 2, 3, 4$ denoting the rotor number, L represents the scalar constant length of each UAV's boom, $\mathbf{e}_1 = [1 \ 0 \ 0]^T$, $\alpha_i(t)$ is the variable tilting angle and $\chi = \left\{\frac{\pi}{4}, \frac{3\pi}{4}, -\frac{3\pi}{4}, -\frac{\pi}{4}\right\}$ is the set of constant orientations of each rotor about ${}^B z_{R_i}$ axis, whereas $R_.(\cdot) \in SO(3)$ are the rotation matrices. Furthermore, each rotor's thrust and drag torque are regarded to its corresponding propeller's aerodynamic parameters by

$$T_i \in \mathbb{R} \triangleq k_f \omega_i^2, \tag{4}$$

and

$$\tau_{d_{R_i}} \in \mathbb{R} \triangleq k_\tau \omega_i^2, \tag{5}$$

where k_f and k_τ the scalar positive constant coefficients related to the propellers geometry and $\omega_i \in \mathbb{R}$ is the $i-$th rotor angular velocity. Thus, each propeller exerts the forces $f_{R_i} \in \mathbb{R}^3$ and torques $\tau_{R_i} \in \mathbb{R}^3$ according to its position and orientation as follows

$$f_{R_i} = T_i {}^B R_{R_i}(\alpha_i(t))\mathbf{e}_3, \tag{6}$$

$$\tau_{R_i} = {}^B p_{R_i} \times T_i {}^B R_{p_i}(\alpha_i(t)) + (-1)^{i-1} \tau_{d_{R_i}} {}^B R_{p_i}(\alpha_i(t))\mathbf{e}_3, \tag{7}$$

where $\mathbf{e}_3 = [0 \ 0 \ 1]^T$. Notice that the control wrench $u_B \in \mathbb{R}^6$ can be split into control forces $u_f^B \in \mathbb{R}^3$ and control torques

$u_\tau^B \in \mathbb{R}^3$, which are related to the propeller forces and torques by

$$u_B = \begin{bmatrix} u_f^{B^T} & u_\tau^{B^T} \end{bmatrix}^T = \begin{bmatrix} \sum_{i=1}^4 f_{R_i}^T & \sum_{i=1}^4 \tau_{R_i}^T \end{bmatrix}^T . \quad (8)$$

Therefore, from (6), (7) and (8) the following relation can be obtained

$$u_B = k_f \Lambda \Omega, \quad (9)$$

where $\Lambda \in \mathbb{R}^{4\times 8}$ is the allocation matrix expressed as

$$\Lambda = \begin{bmatrix} 0 & 0 & 0 & 0 & \frac{1}{\sqrt{2}} & \frac{1}{\sqrt{2}} & -\frac{1}{\sqrt{2}} & -\frac{1}{\sqrt{2}} \\ 0 & 0 & 0 & 0 & -\frac{1}{\sqrt{2}} & \frac{1}{\sqrt{2}} & \frac{1}{\sqrt{2}} & -\frac{1}{\sqrt{2}} \\ 1 & 1 & 1 & 1 & 0 & 0 & 0 & 0 \\ \frac{L}{\sqrt{2}} & \frac{L}{\sqrt{2}} & -\frac{L}{\sqrt{2}} & -\frac{L}{\sqrt{2}} & \frac{\sigma}{\sqrt{2}} & -\frac{\sigma}{\sqrt{2}} & -\frac{\sigma}{\sqrt{2}} & \frac{\sigma}{\sqrt{2}} \\ -\frac{L}{\sqrt{2}} & \frac{L}{\sqrt{2}} & \frac{L}{\sqrt{2}} & -\frac{L}{\sqrt{2}} & -\frac{\sigma}{\sqrt{2}} & -\frac{\sigma}{\sqrt{2}} & \frac{\sigma}{\sqrt{2}} & \frac{\sigma}{\sqrt{2}} \\ \sigma & -\sigma & \sigma & -\sigma & -L & -L & -L & -L \end{bmatrix},$$

with $\sigma = k_f/k_\tau$, and

$$\Omega \in \mathbb{R}^8 \triangleq \begin{bmatrix} T_{1_z} & T_{2_z} & T_{3_z} & T_{4_z} & T_{1_{xy}} & T_{2_{xy}} & T_{3_{xy}} & T_{4_{xy}} \end{bmatrix}^T .$$

Finally, it is possible to map any control wrench u_B to the required rotor speeds and tilting angles of the omnidirectional quadrotor using

$$\Omega = \Lambda^+ u_B, \quad (10)$$

$$T_i = \sqrt{T_{i_z}^2 + T_{i_{xy}}^2}, \quad (11)$$

$$\omega_i = \sqrt{\frac{T_i}{k_f}}, \quad (12)$$

and

$$\alpha_i(t) = tan^{-1}\left(\frac{T_{i_z}}{T_{i_{xy}}}\right), \quad (13)$$

where Λ^+ denotes the pseudoinverse of Λ.

III. Hybrid Force/Position Control

Active interaction control can be classified into direct and indirect force control, the former performs the control action through motion control without a force feedback loop, whereas the latter uses the feedback loop to control the contact wrench [13]. Impedance and admittance controllers fall within the indirect approach for instance, meanwhile hybrid force/motion control is a widely used direct force technique that allows controlling both contact wrench and end-effector motion simultaneously [13]. In the context of aerial manipulators, hybrid force/motion has been successfully applied in a parallel configuration, where the contact force and position controllers are conducted separately as constrained and free-flight spaces [11]. On the other hand, a different architecture that allows specifying the force and motion-controlled axes has been developed in [14], but up to the best authors' knowledge, it has not been applied to aerial manipulators. Thus, inspired by such a control approach for ground-fixed manipulators and exploiting the robust motion controller presented in [12], the following controller is proposed

$$\begin{cases} u_B = & (I_{6\times 6} - S)\left[K_p \tanh\left(\tilde{\boldsymbol{\zeta}}\right) + K_i \tanh\left(\xi\right)\right] + K_v \dot{\tilde{\zeta}} \\ & + S\left[K_f \tilde{f} + K_j \varphi\right] , \\ \dot{\xi} = & \tilde{\zeta} , \\ \dot{\varphi} = & \tilde{f} , \end{cases} \quad (14)$$

where $\tilde{\zeta} \in \mathbb{R}^6 \triangleq \zeta^d - \zeta$ is the pose error with ζ^d defined as a constant vector, $\tilde{f} \in \mathbb{R}^6 \triangleq f^d - f$ is the force error with f^d defined as a constant vector as well, $K_p,\ K_i,\ K_v,\ K_f,\ K_j \in \mathbb{R}^{6\times 6}$ are diagonal matrices with positive entries and $S \in \mathbb{R}^{6\times 6}$ is a switching matrix composed of zeros and ones that specify which axes are force-controlled. Since the target of this work is to deliver horizontal sustained force along x_B axis, then the switching matrix is chosen as $S = \text{diag}(1,0,0,0,0,0)$ when the aerial manipulator reaches the desired application point $x_0 \in \mathbb{R}$, hence the force control part along such an axis is given by

$$\begin{cases} u_{B_x} = & k_{f_x}\tilde{f}_x + k_{j_x}\varphi_x + k_{v_x}\dot{\tilde{\zeta}}_x , \\ \dot{\varphi}_x = & \tilde{f}_x , \end{cases} \quad (15)$$

where each term $\cdot_x$ represents the scalar $x-$axis component of the corresponding vector in (14) and $k_{f_x},\ k_{j_x},\ k_{v_x}$ are positive constants contained in the first entry of $K_f,\ K_j$ and K_v respectively.

A. Stability of the Force Control Loop

The global asymptotic stability of the motion controller part of (14) has been proved in [12]. Besides, it is assumed that the horizontal force is performed with zero orientation, namely ${}^W\eta_B = 0_3$. Furthermore, it is also assumed that all the axes except for x_B are stably position-controlled and that the horizontal force is delivered to a completely rigid environment. Hence the horizontal motion dynamics along x_B is given by

$$m\ddot{\zeta}_x = u_{B_x}. \quad (16)$$

Now, the tuning parameters for the controller (15) are defined as $k_{j_x} = k_{f_x}/\lambda$ and $k_{v_x} = m/\lambda$, with the scalar $\lambda > 0$, as well as the auxiliary variable

$$s = k_{f_x}\varphi_x - m\dot{\zeta}_x . \quad (17)$$

Based in the aforesaid considerations, the following Theorem states the global asymptotic stability.

Theorem 1. *Considering that the motion controlled axes are stably regulated about a desired set point, then the force error $\tilde{f}_x \to 0$ asymptotically as $t \to \infty$ through the direct force controller* (15)*.*

Proof. The following Lyapunov candidate function $V(s) = s^2/2$ is proposed, whose time derivative is

$$\dot{V}(s) = s\dot{s} = s\left(k_{f_x}\tilde{f}_x - m\ddot{\zeta}_x\right) = s\left(k_{f_x}\tilde{f}_x - u_{B_x}\right) .$$

Therefore,

$$\dot{V}(s) = s\left(k_{f_x}\tilde{f}_x - k_{f_x}\tilde{f}_x - k_{j_x}\varphi_x - k_{v_x}\dot{\tilde{\zeta}}_x\right) .$$

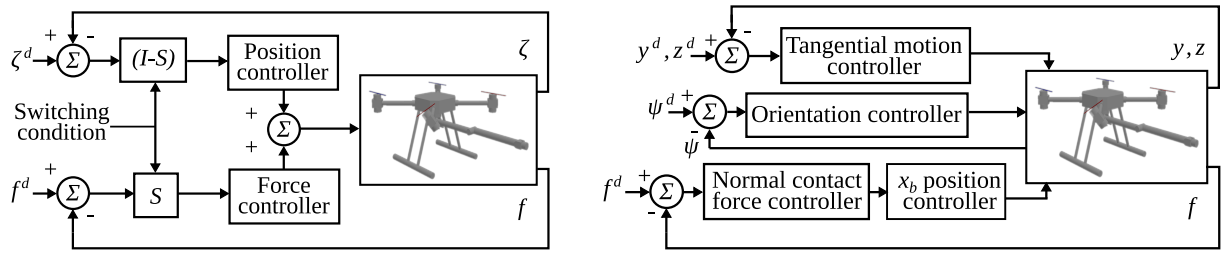

(a) (b)

Fig. 2: Control schemes: (a) proposed controller block diagram. (b) Simplified controller block diagram presented in [11].

Taking into account $\dot{\zeta}_x^d = 0$ and the tuning parameter λ, then

$$\dot{V}(s) = \frac{1}{\lambda} s \left(-k_{f_x} \varphi_x + m \dot{\zeta}_x \right) = -\frac{1}{\lambda} s^2 \ .$$

Hence, the asymptotic convergence of s to zero is guaranteed as $t \to \infty$. Notice that the motion of the UAV is constrained along ζ_x after the contact with the rigid environment is established at the constant point x_0, so $\dot{\zeta}_x = 0$. Therefore, if $s \to 0$ then $\varphi_x \to 0$ and consequently, $\dot{\varphi_x} = \tilde{f}_x \to 0$ asymptotically as well.

□

TABLE I: Parameters of the actively tilting quadrotor dynamics and allocation matrix.

Parameter	Value
m	$5\,\text{kg}$
J_b	$\text{diag}(0.1522, 0.1522, 0.1841)\,\text{kg m}^2$
g	$9.81\,\text{m/s}^2$
l	0.183847763
k_f	8.54858×10^{-5}
k_τ	1.75×10^{-4}
k_{f_x}	0.01
k_{j_x}	0.005

IV. Physics-engine Based Simulation Results

To assess the effectiveness of the proposed controller (14), the physics-engine-based simulator *Gazebo* was implemented, which yields results very close to experiments with actual UAVs as a consequence of the several physics phenomena included by default.

The execution of the hybrid force/position control system was achieved by way of three programs, the position control algorithm developed in C++ and the Python-based force control and navigation algorithms. The controller input and output signals were communicated with the virtual aerial manipulator through *ROS* messages. The parameters of the actively tilting quadrotor dynamics and allocation matrix are presented in TABLE I. The block diagram of the presented hybrid force/position control is depicted in Fig. 2a, where it can be appreciated the decoupled architecture as is proposed by [14] for ground-fixed manipulators.

The proposed controller of this work was contrasted against the state-of-the-art force control with the inner position control loop presented in [11], whose simplified block diagram is illustrated in Fig. 2b. The x_B position control is given by

$$\begin{cases} x_B^d &= x_B^d + k_{f_x} \tilde{f}_x + k_{j_x} \varphi_x, \\ \dot{\varphi}_x &= \tilde{f}_x. \end{cases} \tag{18}$$

It can be noticed that this hybrid approach is a completely different architecture than the proposed, besides it does not exploit the thrust vectoring provided by the actively tilting propellers, so the proposed architecture in this work is completely novel concerning the aerial manipulators.

The following experiments were conducted. Firstly, the aerial manipulator was commanded to deliver a set of five different desired horizontal forces along x_B to a rigid object, for one minute each, using the force control with inner position control loop as is shown in Fig. 4. Next, the proposed controller of this work was implemented, likewise, using the same set of forces to be tracked. The obtained results were compared by plots and a performance index. A brief video showing how the experiments were put into effect is available at https://youtu.be/Hdn0EmdPxBA.

Fig. 3a shows the results using the force controller (18), where it can be observed that the force is controlled correctly up to 4 N; beyond such a force, the controller is not able anymore to track the set point.

On the other hand, the results using the proposed controller of this work are presented in Fig. 3b, where it can be appreciated that the force is regulated, with some oscillations but correctly, up to 8 N.

To provide a quantitative comparison, the root-mean-squared error (RMSE) for each set of experiments was computed using

$$RMSE = \sqrt{\frac{\sum_{k=1}^{N} \tilde{f}_{x_k}^2}{N}}. \tag{19}$$

The position-based controller RMSE yielded 0.8609, meanwhile, the hybrid technique RMSE obtained was 0.3782, showing an advantage in favor of the latter.

V. Conclusions

In summary, the paper introduces a hybrid force/position controller tailored for aerial manipulators equipped with tilting propellers, evaluated within the *Gazebo* physics-engine-based simulator. Compared to a state-of-the-art force control method, the proposed controller demonstrates superior performance by effectively sustaining forces of up to 8 N, surpassing the 5 N limit of the comparator. Quantitative analysis employing root-mean-squared error (RMSE) favors the proposed hybrid

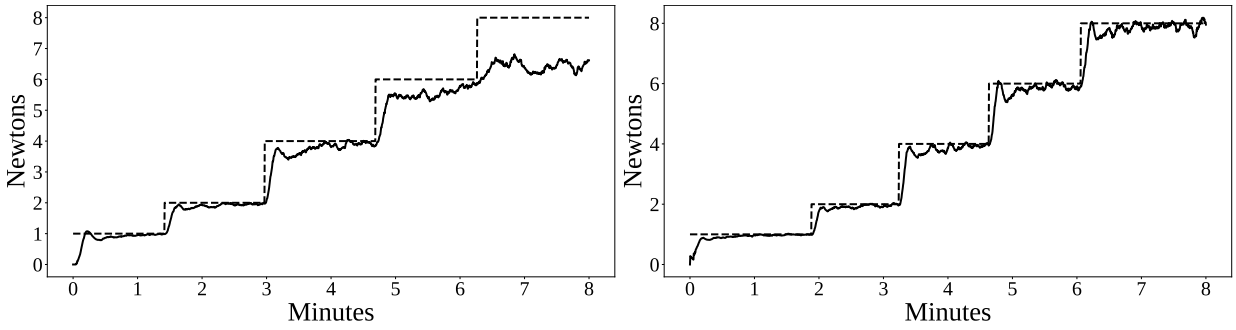

(a) (b)

Fig. 3: Experimental results: case study (a) force control results using the inner-position-loop force controller (18); case study (b) force control results using the hybrid position/force control (14)- (15).
- - - Desired force. —- Measured force.

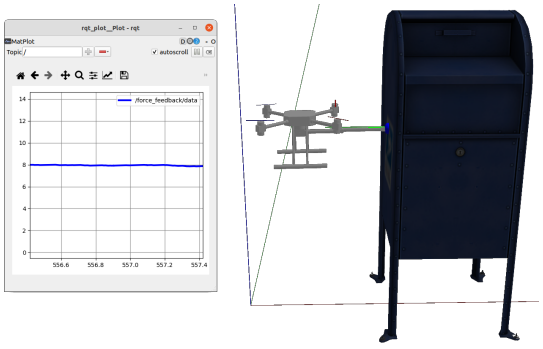

Fig. 4: Aerial manipulator delivering an 8 N force to a rigid object.

system, exhibiting a 56% lower error (0.3782) compared to the position-based controller (0.8609). These findings underscore the efficacy and precision of the proposed controller for regulating forces in aerial manipulation tasks. The contributions presented in this paper hold promise various applications of aerial manipulator such as, cleaning of tall buildings/towers, push and slide operations, picking and placing objects, executing precise peg-in-hole tasks, infrastructure repairing, painting and maintenance. Moreover, their ability to operate in hazardous environments makes them invaluable tools for critical tasks like search and rescue operations.

Future research directions may include real-world experiments with physical UAVs to validate simulation results. Additionally, exploring adaptive control strategies and integrating advanced sensing technologies could enhance the system's robustness and applicability in dynamic environments. The potential impact of the proposed controller across various aerial manipulation applications positions it as a promising avenue for ongoing research and development.

ACKNOWLEDGEMENTS

The research leading to these results has been supported by the AEROT-RAIN Project, European Union's Horizon 2020 Research and Innovation Program under the Marie Skłodowska-Curie Grant Agreement 953454. The authors are solely responsible for its content.

REFERENCES

[1] F. Ruggiero, V. Lippiello, and A. Ollero, "Aerial manipulation: A literature review," *IEEE Robotics and Automation Letters*, vol. 3, no. 3, pp. 1957–1964, 2018.

[2] S. Darvishpoor, J. Roshanian, A. Raissi, and M. Hassanalian, "Configurations, flight mechanisms, and applications of unmanned aerial systems: A review," *Progress in Aerospace Sciences*, vol. 121, p. 100694, 2020.

[3] N. Ahmed and M. Chen, "Sliding mode control for quadrotor with disturbance observer," *Advances in Mechanical Engineering*, vol. 10, no. 7, p. 1687814018782330, 2018.

[4] J. Cacace, S. M. Orozco-Soto, A. Suarez, A. Caballero, M. Orsag, S. Bogdan, G. Vasiljevic, E. Ebeid, J. A. A. Rodriguez, and A. Ollero, "Safe local aerial manipulation for the installation of devices on power lines: Aerial-core first year results and designs," *Applied Sciences*, vol. 11, no. 13, p. 6220, 2021.

[5] M. Mohammadi, D. Bicego, A. Franchi, D. Barcelli, and D. Prattichizzo, "Aerial tele-manipulation with passive tool via parallel position/force control," *Applied Sciences*, vol. 11, no. 19, p. 8955, 2021.

[6] V. Lippiello and F. Ruggiero, "Cartesian impedance control of a uav with a robotic arm," *IFAC Proceedings Volumes*, vol. 45, no. 22, pp. 704–709, 2012.

[7] S. D'Angelo, A. Corrado, F. Ruggiero, J. Cacace, and V. Lippiello, "Stabilization and control on a pipe-rack of a wheeled mobile manipulator with a snake-like arm," *Robotics and Autonomous Systems*, vol. 171, p. 104554, 2024.

[8] S. D'Angelo, F. Pagano, F. Ruggiero, and V. Lippiello, "Development of a control framework to autonomously install clip bird diverters on high-voltage lines," in *2023 International Conference on Unmanned Aircraft Systems (ICUAS)*, pp. 377–382, 2023.

[9] S. M. Orozco-Soto, E. Cuniato, J. Cacace, M. Selvaggio, F. Ruggiero, V. Lippiello, and B. Siciliano, "Aerial manipulator interaction with the environment," in *Control of Autonomous Aerial Vehicles: Advances in Autopilot Design for Civilian UAVs*, pp. 319–347, Springer, 2023.

[10] D. Lee, H. Seo, D. Kim, and H. J. Kim, "Aerial manipulation using model predictive control for opening a hinged door," in *2020 IEEE International Conference on Robotics and Automation (ICRA)*, pp. 1237–1242, IEEE, 2020.

[11] X. Meng, Y. He, and J. Han, "Hybrid force/motion control and implementation of an aerial manipulator towards sustained contact operations," in *2019 IEEE/RSJ International Conference on Intelligent Robots and Systems (IROS)*, pp. 3678–3683, IEEE, 2019.

[12] S. M. Orozco Soto, F. Ruggiero, and V. Lippiello, "Globally attractive hyperbolic control for the robust flight of an actively tilting quadrotor," *Drones*, vol. 6, no. 12, p. 373, 2022.

[13] L. Villani, "Force control in robotics," in *Encyclopedia of Systems and Control*, pp. 827–833, Springer, 2021.

[14] M. H. Raibert and J. J. Craig, "Hybrid position/force control of manipulators," *Journal of Dynamic Systems, Measurement and Control*, vol. 103, no. 2, pp. 126–133, 1981.